Source Mechanism from Spectrums of Long-Period Surface Waves

2. The Kamchatka Earthquake of November 4, 1952[1]

ARI BEN-MENAHEM AND M. NAFI TOKSÖZ

California Institute of Technology, Seismological Laboratory, Pasadena

Abstract. Fourier analysis of mantle Love and Rayleigh waves from the source of the Kamchatka earthquake of November 4, 1952, recorded on the Benioff linear strain seismograph at Pasadena, furnished further evidence in support of the moving-source theory. Amplitude and phase spectrums of G_1, G_2, G_3, G_4, R_2, and R_3 were processed to obtain information on the mechanism at the source. Both the directivity and the differential phase agree on a unilateral fault of 700 km which ruptured with a speed of 3 km/sec in the direction N 146° W. The fault length is in good agreement with the extent of aftershock distribution in the month of November 1952. The initial phases of Love and Rayleigh waves agree on a mechanism of a right orthogonal double couple with a time dependence which is close to the Heaviside step function.

Introduction. In previous work [*Ben-Menahem and Toksöz,* 1962], the source mechanism of the Mongolian earthquake of December 4, 1957, was obtained from the Fourier spectrums of Rayleigh waves recorded at Pasadena. In the present paper a study of the source mechanism is reported, using both the Rayleigh and the Love waves. We are able to derive not only the dynamic parameters of fault length and rupture speed, but also the initial time function and the force system.

The Kamchatka earthquake occurred on November 4, 1952, 16h 58m 22s UT at the initial epicenter, 52.6°N, 160.3°E [I.S.S.]. The Richter magnitude was 8¼. This earthquake had been associated with first observation of the free oscillations of the earth [*Benioff,* 1958] and first studies of the structure of the upper mantle by means of long-period surface waves [*Ewing and Press,* 1954]. It was also studied in connection with aftershock distribution [*Hutchinson,* 1954; *Båth and Benioff,* 1958], propagation of G waves [*Satô,* 1958], and direction of faulting [*Hodgson,* 1956].

In our analysis we used the N-S and E-W components of the Pasadena linear strain seismograph. The original seismograms are shown in Figures 1 and 2. The signal R_3 on the N-S component could not be retraced without ambiguity and was therefore discarded.

Preparatory operations on the time series. The data pertinent to the analyzed signals are shown in Table 1. Each wave train was digitized at equal intervals of 2 seconds and Fourier analyzed on the Caltech IBM 7090 electronic computer. Prior to the Fourier analysis, the traces were filtered with a low-pass digital filter. A typical filter response is given in Figure 3.

Distances over the earth's surface were computed for the international ellipsoid using Rudo's formula [*Bomford,* 1952]. Geodesics have been approximated by normal sections. The error due to this approximation is less than 1 meter, and is probably smaller than the deviation of the international ellipsoid from the geoid. Azimuths and central angles were computed from formulas of *Bullen* [1947]. t_n in Table 1 is the time delay of the signal onset with reference to the time of origin of the earthquake. In these computations a program written by *Alexander* [1963] was used.

The position of Pasadena relative to the source of the earthquake is shown in Figure 4. The original separated traces of the signals are shown in Figures 5, 6, 7, and 8. Some filtered signals are given in Figure 9.

The entire scheme of the data processing is shown in Figure 10. To begin with, auxiliary data such as time of origin and initial epicenter are used to obtain the station-to-epicenter geometry and the expected arrivals of the various Love and Rayleigh phases. Once the signals are located and found to have a sufficient amount of power in the spectral region of interest, they

[1] Contribution 1146, Division of Geological Sciences, California Institute of Technology, Pasadena.

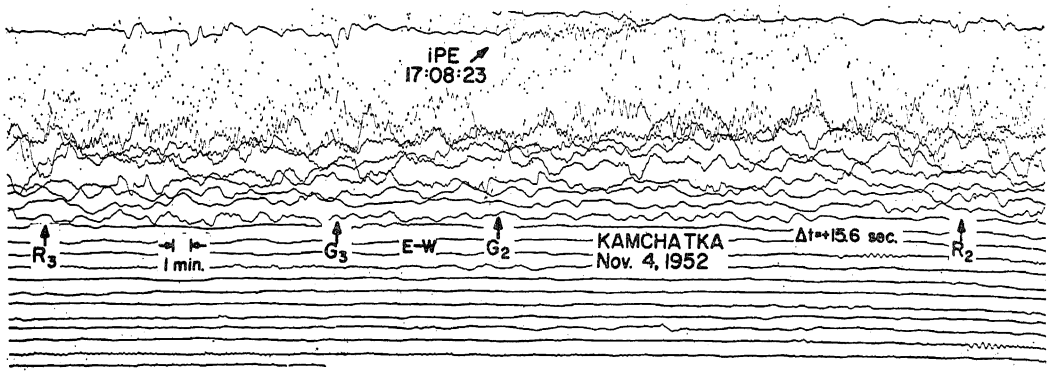

Fig. 1. The Pasadena E-W linear strain record ($T_g = 70$ sec) of the Kamchatka earthquake.

are checked for purity by consulting conventional dispersion and travel-time curves. Possible interference with body waves and higher modes of surface waves have to be checked carefully before the Fourier analysis. After the analysis the phase velocities and the attenuation coefficients are compared with known data for similar paths. It is always advantageous to perform the Fourier analysis for various sizes of windows for each signal and compare the resulting spectrums. Next, the resulting phase spectrums are used in pairs to compute the phase velocities. Figure 11 shows curves for phase and group velocities of the fundamental Love and Rayleigh modes. Measurements of phase velocities have been reported in detail elsewhere [*Toksöz and Ben-Menahem*, 1963].

Theoretical model. Ben-Menahem [1960] investigated the effect of the source finiteness on radiation of seismic waves from simple models of fault planes. The integrated displacement spectrum from a strike-slip fault of length b, moving with a velocity V is given by

$$u_\theta = \frac{A_\theta(\theta)}{\sqrt{r}} \frac{\sin X}{X} L(\omega) N_\theta(\omega, h) \cdot \exp i\left[\omega\left(t - \frac{r}{c}\right) - X + m\frac{\pi}{2} + \delta + \epsilon_\theta\right] \quad (1)$$

$$u_r = \frac{A_r(\theta)}{\sqrt{r}} \frac{\sin X}{X} L(\omega) N_{rr}(\omega, h) \cdot \exp i\left[\omega\left(t - \frac{r}{c}\right) - X + m\frac{\pi}{2} + \delta + \epsilon_r\right] \quad (2)$$

$$u_z = \frac{A_z(\theta)}{\sqrt{r}} \frac{\sin X}{X} L(\omega) N_{zr}(\omega, h) \cdot \exp i\left[\omega\left(t - \frac{r}{c}\right) - X + m\frac{\pi}{2} + \delta + \epsilon_z\right] \quad (3)$$

where (u_θ, u_r, u_z) is the displacement vector in a cylindrical coordinate system with the initial epicenter at the origin and the station at a point (r,θ) on the free surface. The fault is pointing

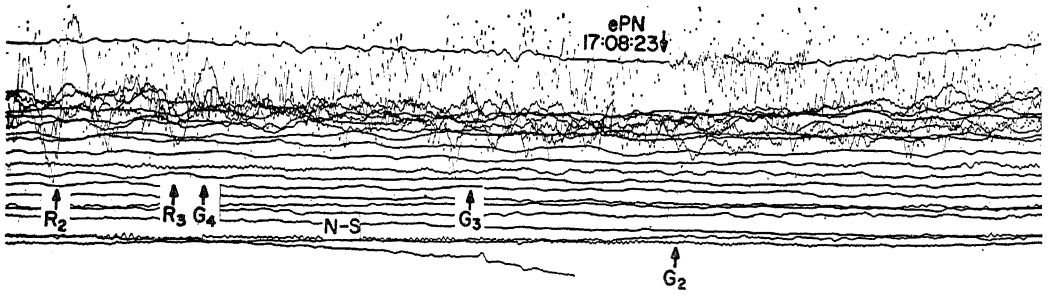

Fig. 2. The Pasadena N-S linear strain record ($T_g = 70$ sec) of the Kamchatka earthquake.

TABLE 1. The Digitized Signals Recorded on the Linear Strain Seismograph at Pasadena, California (34°08′54″N, 118°10′18″W)

Signal	Component	Period of Galvanometer	Distance Traveled, km	Onset of Wave h	m	s	t_n, sec	Group Velocity Window, km/sec Begin	End	Record Length, sec
R_2	N-S	70	33,493	19	19	06	8444	3.97	3.47	1200
R_2	E-W	70	33,493	19	18	54	8432	3.97	3.45	1266
R_3	E-W	70	46,571	20	14	06	11744	3.96	3.41	1914
G_1	N-S	180	6,539	17	20	16	1314	4.97	3.90	360
G_2	N-S	180	33,493	19	00	16	7314	4.58	4.08	900
G_2	N-S	70	33,493	19	05	07	7605	4.40	4.22	320
G_2	E-W	70	33,493	19	04	31	7569	4.42	4.20	402
G_3	N-S	70	46,571	19	51	06	10364	4.49	4.19	740
G_3	E-W	70	46,571	19	51	54	10412	4.47	4.17	762
G_4	N-S	70	73,525	21	35	07	16605	4.43	4.26	654

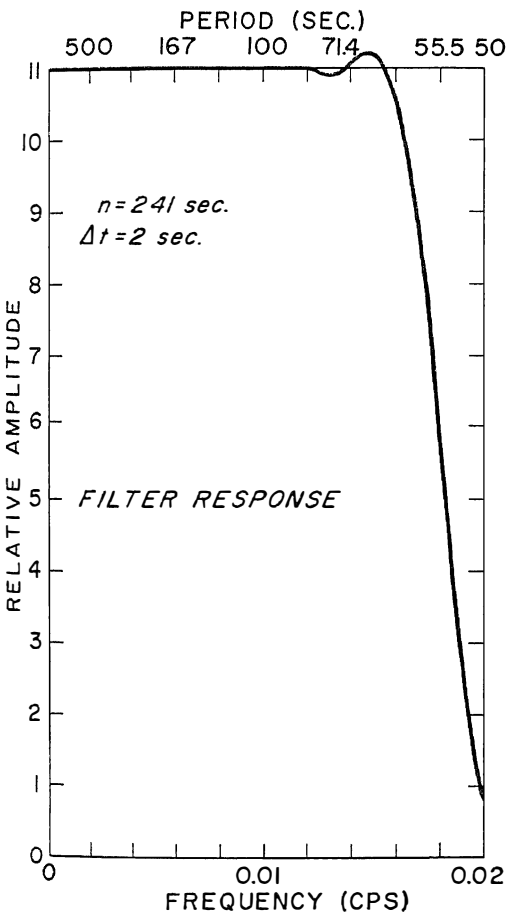

Fig. 3. Response of the digital filter used to eliminate high-frequency noise from the digitized signals.

in the X direction, θ is measured positively counterclockwise, and the z axis is chosen positive *upward*. θ_0 is the angle between the fault line and the line from the source to the station; it is taken positive in counterclockwise direction when observed from above the half-space. u_θ is the Love wave displacement and u_r and u_z are the components of the Rayleigh wave motion. The amplitude response functions of the elastic medium, $N_\theta(\omega,h)$, $N_{rr}(\omega,h)$, and $N_{zr}(\omega,h)$, can be obtained explicitly by solving the wave equation for a layered medium with a directional source in one of the layers. $m(\pi/2)$ is the polar phase shift of surface waves for m polar passages [*Brune et al.*, 1961].

The source is assumed to be specified as a product of three factors: (1) *The spatial factor* $A(\theta)e^{i\epsilon}$, which depends on the force system, (2) *the temporal factor* $L(\omega)e^{i\delta(\omega)}$, which is the Fourier transform of the source time function, and (3) *the propagation factor* $(\sin X/X)e^{-iX}$, where $X = \omega b/2c\ (c/v - \cos\theta_0)$, which arises from the assumption that the rupture along the fault is moving horizontally with a uniform speed V along a segment of length b.

The values of the spatial factors for three elementary force systems, the single force, the couple (dipole with moment), and the orthogonal double couple (obtained by the superposition of two couples at 90°), are listed in Table 2. Some of the cases given in this table were discussed in detail by *Aki* [1962]. The case of the double couple was treated recently by *Haskell* [1963].

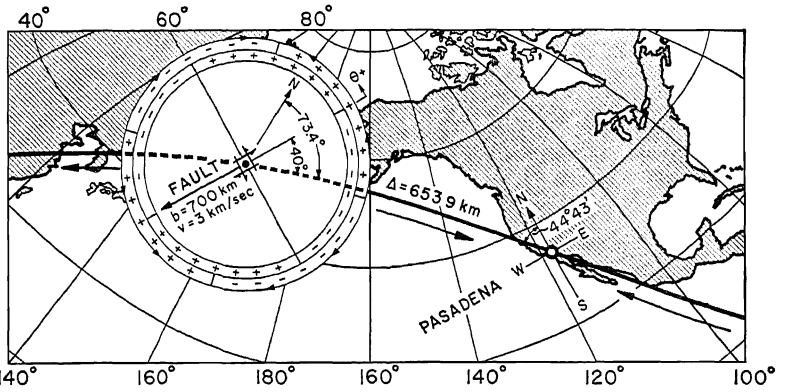

Fig. 4. Position of Pasadena relative to the source of the Kamchatka earthquake. Black line indicates part of geodesic, traveled by surface waves.

We will now show how to construct the far displacement field for an *arbitrary* force system. Consider an orthogonal coordinate system and let a unit force $\mathbf{R}$ be applied to the origin of this system. $\mathbf{R}$ may be written in the form $\mathbf{R} = a\mathbf{e}_1 + b\mathbf{e}_2 + c\mathbf{e}_3$, where $\mathbf{e}_1$, $\mathbf{e}_2$, and $\mathbf{e}_3$ are unit vectors along the x_1, x_2, and x_3 axes, and a, b, and c are the direction cosines of $\mathbf{R}$. Let the displacement vector at a station P due to the unit force $\mathbf{e}_j$ be (u_j, v_j, w_j). The total displacement $\mathbf{U}_s$ due to $\mathbf{R}$ may then be expressed as

$$\begin{aligned}\mathbf{U}_s = {} & (au_1 + bu_2 + cu_3)\mathbf{e}_1 \\ & + (av_1 + bv_2 + cv_3)\mathbf{e}_2 \\ & + (aw_1 + bw_2 + cw_3)\mathbf{e}_3 \qquad (4)\end{aligned}$$

The displacements $\mathbf{U}_c$ due to a couple are obtained from the singlet displacements $\mathbf{U}_s$ by differentiating the vector $\mathbf{U}_s$ in the direction of the couple arm. Let $\mathbf{S}$ be a unit vector along the arm of the couple formed by $\mathbf{R}$, then $\mathbf{U}_c = (\mathbf{S}\cdot\nabla)\mathbf{U}_s$. Expressing the operator ∇ by the coordinates (r, θ, z) of the point of observation with respect to the fixed source, we obtain

$$\begin{aligned}\mathbf{U}_c = {} & \left[\cos(\mathbf{r}, \mathbf{s})\frac{\partial}{\partial r} + \frac{\sin(\mathbf{r}, \mathbf{s})}{r}\frac{\partial}{\partial \theta}\right. \\ & \left. + \cos(\mathbf{e}_z, \mathbf{s})\frac{\partial}{\partial z}\right]\mathbf{U}_s \qquad (5)\end{aligned}$$

To derive the displacement field of a double-couple source we first define the vectors $\mathbf{F}_1(u_1, u_2, u_3)$, $\mathbf{F}_2(v_1, v_2, v_3)$, and $\mathbf{F}_3(w_1, w_2, w_3)$, and rewrite the singlet displacement vec-

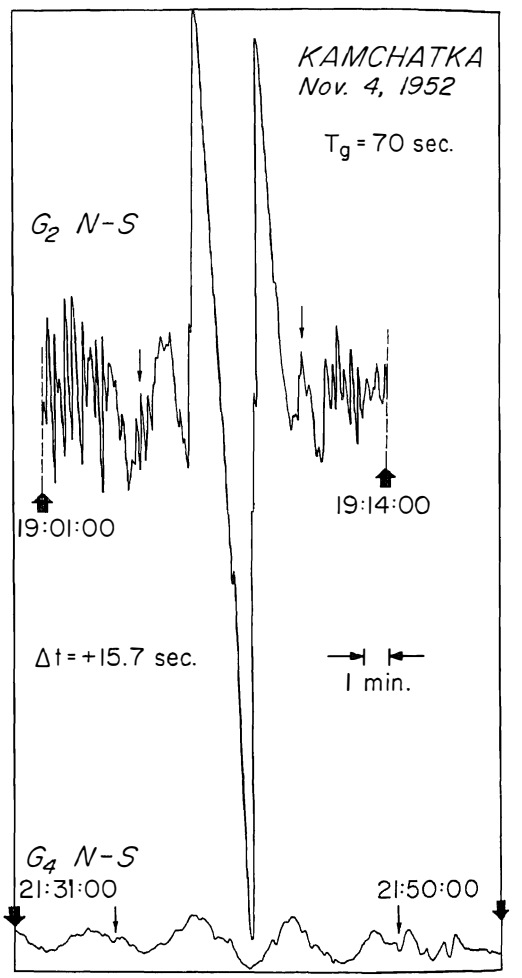

Fig. 5. The unfiltered traces of mantle Love waves G_2 and G_4, N-S (T_g = 70 sec), of the Kamchatka earthquake.

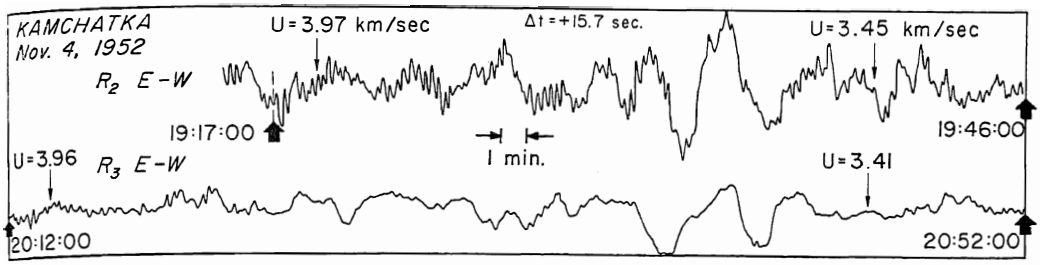

Fig. 6. The unfiltered traces of mantle Rayleigh waves R_2 and R_3, E-W ($T_g = 70$ sec), of the Kamchatka earthquake.

tor in the form $\mathbf{U}_s = (\mathbf{R}\cdot\mathbf{F}_1)\mathbf{e}_1 + (\mathbf{R}\cdot\mathbf{F}_2)\mathbf{e}_2 + (\mathbf{R}\cdot\mathbf{F}_3)\mathbf{e}_3$. Substituting this representation into the equation $\mathbf{U}_c = (\mathbf{S}\cdot\nabla)\,\mathbf{U}_s$, we obtain $\mathbf{U}_c = [\mathbf{R}\cdot(\mathbf{S}\cdot\nabla)\mathbf{F}_1]\mathbf{e}_1 + [\mathbf{R}\cdot(\mathbf{S}\cdot\nabla)\mathbf{F}_2]\mathbf{e}_2 + [\mathbf{R}\cdot(\mathbf{S}\cdot\nabla)\mathbf{F}_3]\mathbf{e}_3$. The double-couple displacements $\mathbf{U}_{dc}$ are obtained by a superposition of the fields of two orthogonal couples. Skipping the intermediate steps, we obtain

$$\mathbf{U}_{dc} = (\mathbf{M}\cdot\nabla \times \mathbf{F}_1)\mathbf{e}_1 + (\mathbf{M}\cdot\nabla \times \mathbf{F}_2)\mathbf{e}_2 + (\mathbf{M}\cdot\nabla \times \mathbf{F}_3)\mathbf{e}_3 \qquad (6)$$

where $\mathbf{M} = (\mathbf{S} \times \mathbf{R})$ is a unit moment vector.

We now consider some useful examples. We may assume without loss of generality that a unit force $\mathbf{R}(\sin\lambda, 0, -\cos\lambda)$ with a moment arm $\mathbf{S}(\alpha, \beta, \gamma)$ is applied at $(0, 0, -h)$. From

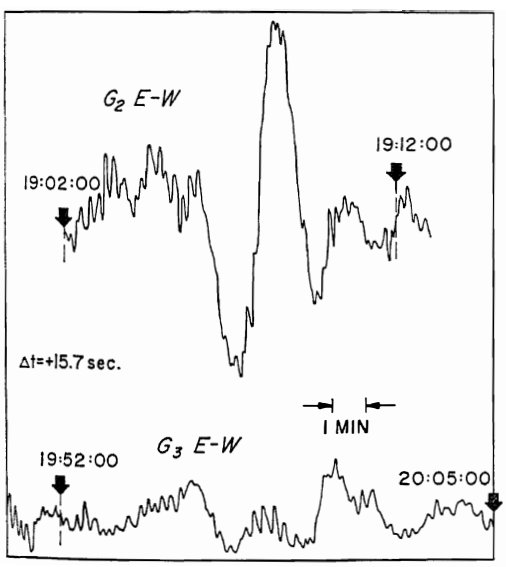

Fig. 7. The unfiltered traces of mantle Love waves G_2 and G_3, E-W ($T_g = 70$ sec), of the Kamchatka earthquake.

(5) and Table 2 we derive the far field of a right couple,

$$U_\theta = e^{-i3\pi/4}\sin\lambda\sin\theta \cdot[(\alpha\cos\theta + \beta\sin\theta) + i\gamma\,\partial/\partial(k_n h)]N_\theta$$

$$U_r = e^{i\pi/4}[(\alpha\cos\theta + \beta\sin\theta) + i\gamma\,\partial/\partial(k_n h)] \cdot[\sin\lambda\cos\theta\,N_{rr} - i\cos\lambda\,N_{zr}] \qquad (7)$$

$$U_z = e^{-i\pi/4}[(\alpha\cos\theta + \beta\sin\theta) + i\gamma\,\partial/\partial(k_n h)] \cdot[\sin\lambda\cos\theta N_{zr} - i\cos\lambda N_{zz}]$$

The functions N_{rz} in (7) are the medium amplitude-response factor due to a force in the positive z direction. The common factor $L(\omega)\exp[i(\omega t - kr) + im(\pi/2) + i\delta]/\sqrt{r}$ is suppressed. Notice that the differentiation with respect to h introduces phase shifts which depend on the polar angle θ.

We now study the case in which $\mathbf{R} = (1, 0, 0)$ and $\mathbf{S} = (0, \sin\delta, -\cos\delta)$. δ is the dip angle. From (7) we find that the spatial phase for this case is

$$\epsilon_\theta = -\frac{3}{4}\pi - \tan^{-1}\left(\frac{q_\theta\cot\delta}{\sin\theta}\right)$$

$$\epsilon_r = \frac{\pi}{4} - \tan^{-1}\left(\frac{q_r\cot\delta}{\sin\theta}\right) \qquad (8)$$

$$\epsilon_z = -\frac{\pi}{4} - \tan^{-1}\left(\frac{q_z\cot\delta}{\sin\theta}\right)$$

where

$$q_\theta = \frac{\partial N_\theta/\partial(k_n h)}{N_\theta} \qquad q_r = \frac{\partial N_{rr}/\partial(k_n h)}{N_{rr}}$$

$$q_z = \frac{\partial N_{rz}/\partial(k_n h)}{N_{rz}} \qquad (9)$$

To derive the far field of a double-couple

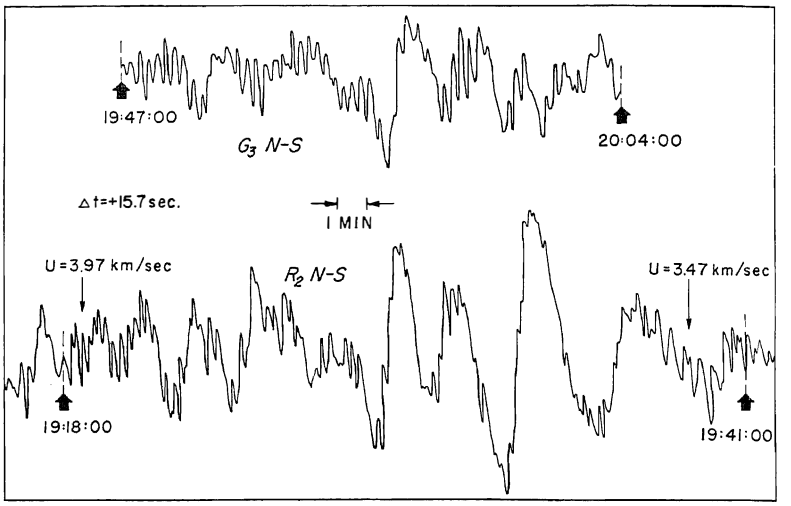

Fig. 8. The unfiltered traces of mantle surface waves G_3, N-S and R_2 N-S ($T_g = 70$ sec), of the Kamchatka earthquake. Amplitude scales are not equal.

source from (6) the operator ∇ is expressed in cylindrical coordinates and the vectors $\mathbf{F}_i$ are obtained from Table 2 in the form

$$\begin{aligned}
\mathbf{F}_\theta &= (\sin\theta e^{i3\pi/4}N_\theta, \\
&\qquad \cos\theta e^{-i\pi/4}N_\theta, 0) \\
\mathbf{F}_r &= (\cos\theta e^{-i\pi/4}N_{rr}, \\
&\qquad \sin\theta e^{-i\pi/4}N_{rr}, e^{i\pi/4}N_{rz}) \qquad (10) \\
\mathbf{F}_z &= (\cos\theta e^{-i3\pi/4}N_{zr}, \\
&\qquad \sin\theta e^{-i3\pi/4}N_{zr}, e^{-i\pi/4}N_{zz})
\end{aligned}$$

The results are straightforward and will not be given here. The double-couple spatial phases for the particular case chosen earlier, will be

$$\begin{aligned}
\epsilon_\theta &= \pi/4 + \tan^{-1}\left(\frac{q_\theta \sin\theta \cot\delta}{\cos 2\theta}\right) \\
\epsilon_r &= \pi/4 + \tan^{-1}\left(\frac{(S_r - q_r)\cot\delta}{2\sin\theta}\right) \qquad (11) \\
\epsilon_z &= -\pi/4 + \tan^{-1}\left(\frac{(S_z - q_z)\cot\delta}{2\sin\theta}\right)
\end{aligned}$$

where $S_r = N_{rz}/N_{rr}$ and $S_z = N_{zz}/N_{rz}$.

Source parameters from amplitude spectrums. Let us now evaluate the fault parameters from R_2 and R_3 of the Kamchatka earthquake of November 4, 1952. The amplitude spectrums of these waves for the period range $250 > T > 50$ sec are shown in Figure 12. Figure 13 shows a comparison between the observed directivity as computed from the amplitude ratio of R_2/R_3 and the theoretical directivity as computed from the function [*Ben-Menahem*, 1960]

$$D = \left|\frac{\left(\frac{C}{V} + \cos\theta_0\right)\left[\sin\frac{\pi b}{CT}\left(\frac{C}{V} - \cos\theta_0\right)\right]}{\left(\frac{C}{V} - \cos\theta_0\right)\left[\sin\frac{\pi b}{CT}\left(\frac{C}{V} + \cos\theta_0\right)\right]}\right| \qquad (12)$$

In this case, the best fit was obtained with the value $b = 700$ km, $V = 3$ km/sec, and $\theta_0 = 140°$. Except for the first maximum, which lies outside our spectral window, the match between the other extremes is satisfactory.

Source mechanism from the phase spectrums.

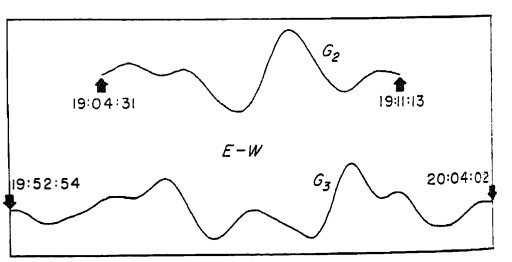

Fig. 9. Mantle Love waves G_2 and G_3 E-W filtered with a low-pass digital filter. Amplitude scales are not equal.

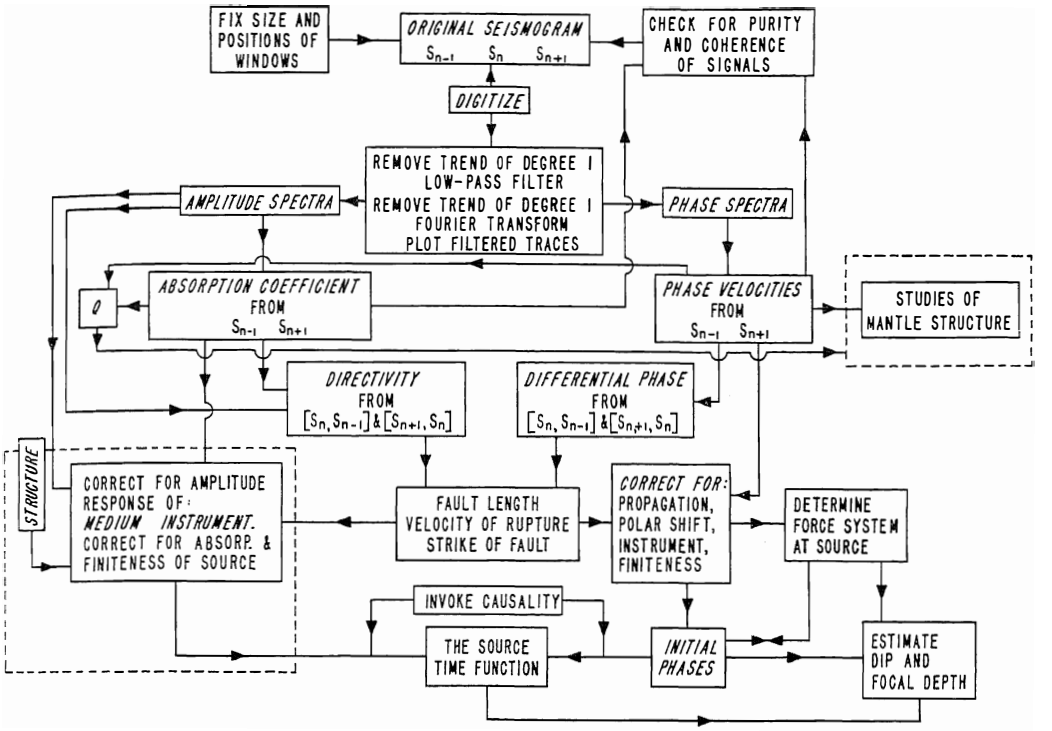

Fig. 10. Data processing routine for study of source mechanism from long-period surface waves. Broken dashed line indicates operations that were not performed in the present study.

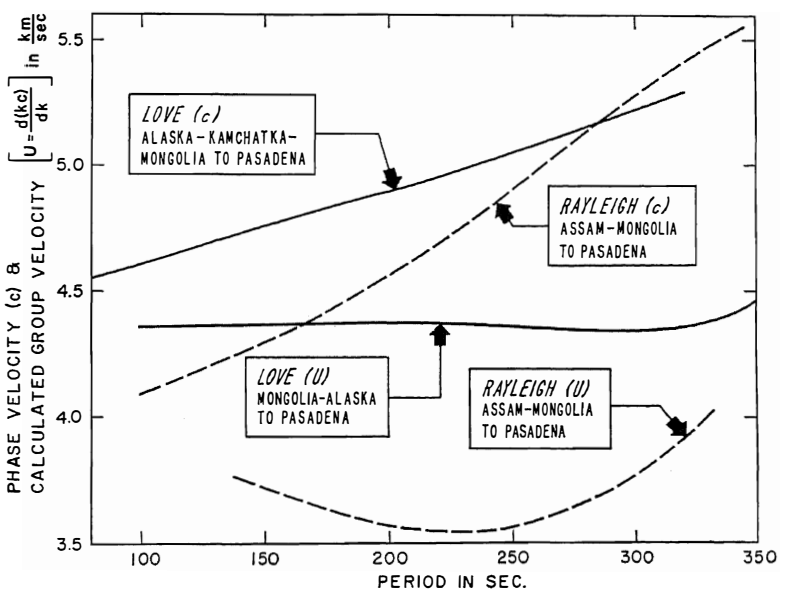

Fig. 11. Phase and group velocities of Love and Rayleigh waves in the period range $80 < T < 350$ sec as measured from records of few major earthquakes recorded at Pasadena, California.

TABLE 2. Spatial Factors of Basic Force Configurations for the Leading Terms of Love and Rayleigh Displacements

Configuration	Symbol	U_θ	U_r	U_z
single force up (+)		0	$e^{i\frac{\pi}{4}}$	$e^{-i\frac{\pi}{4}}$
single force down (-)		0	$e^{-i\frac{3\pi}{4}}$	$e^{i\frac{3\pi}{4}}$
single force east (+)		$\sin\theta e^{i\frac{3\pi}{4}}$	$\cos\theta e^{-i\frac{\pi}{4}}$	$\cos\theta e^{-i\frac{3\pi}{4}}$
single force west (-)		$\sin\theta e^{-i\frac{\pi}{4}}$	$\cos\theta e^{i\frac{3\pi}{4}}$	$\cos\theta e^{i\frac{\pi}{4}}$
left lateral couple (+)		$\sin^2\theta e^{i\frac{\pi}{4}}$	$\sin 2\theta e^{-i\frac{3\pi}{4}}$	$\sin 2\theta e^{i\frac{3\pi}{4}}$
right lateral couple (-)		$\sin^2\theta e^{-i\frac{3\pi}{4}}$	$\sin 2\theta e^{i\frac{\pi}{4}}$	$\sin 2\theta e^{-i\frac{\pi}{4}}$
right orthogonal double couple		$\cos 2\theta e^{i\frac{\pi}{4}}$	$\sin 2\theta e^{i\frac{\pi}{4}}$	$\sin 2\theta e^{-i\frac{\pi}{4}}$
left orthogonal double couple		$\cos 2\theta e^{-i\frac{3\pi}{4}}$	$\sin 2\theta e^{-i\frac{3\pi}{4}}$	$\sin 2\theta e^{i\frac{3\pi}{4}}$

Consider a wave train recorded at a large distance Δ_m from the initial epicenter. It can be represented in the form of a Fourier integral (see equations 2, 3, and 4),

$$F(t) = \int_{-\infty}^{\infty} f(\omega)\, \exp i[\omega t - k\Delta_m + (m-1)\,\pi/2 + \varphi_0 + \varphi_{\text{inst}}]\, d\omega \qquad (13)$$

where $f(\omega)$ is the total spectral amplitude due to the source, the propagation, the absorption, and the instrumental response. φ_0 incorporates space, time, and finiteness phases. φ_{inst} is the instrumental phase shift.

In practice, the inverse operation on the time series at the station is performed with the assumption that $F(t) = 0$ outside the range $t_m < t < t_m + L$, where L is the record length. Hence

$$\int_{-\infty}^{\infty} F(t)e^{-i\omega t}\, dt = e^{-i\omega t_m} \int_0^L F(\tau)e^{-i\omega\tau}\, d\tau \qquad (14)$$

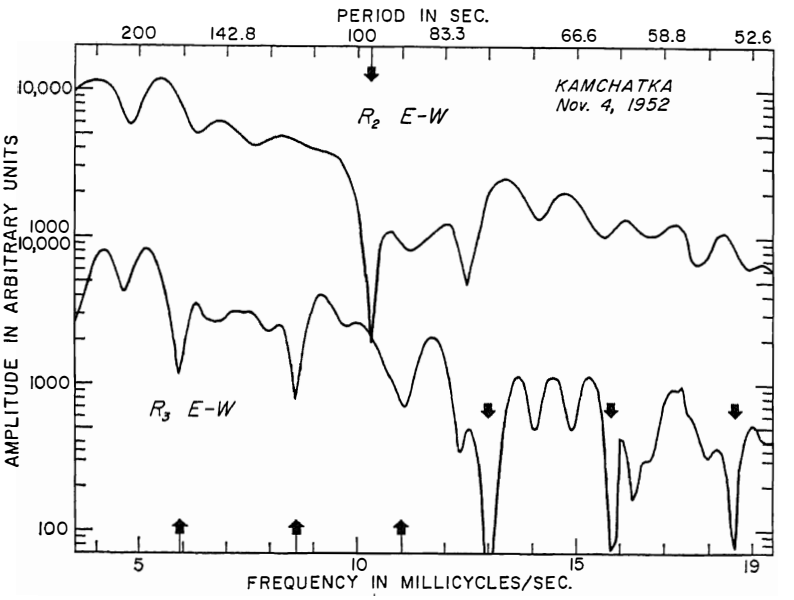

Fig. 12. Amplitude spectrums of mantle Rayleigh waves R_2 and R_3, E-W.

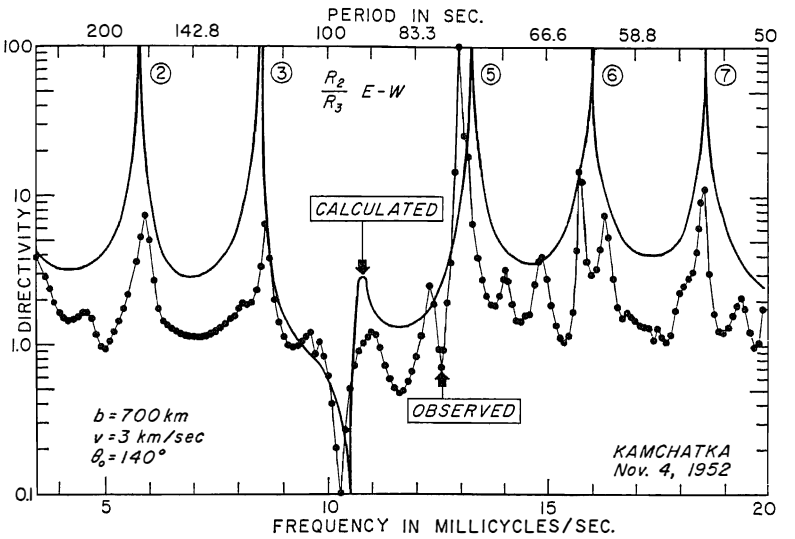

Fig. 13. Observed versus calculated directivity for mantle Rayleigh waves R_2/R_3 on a semilog scale.

where t_m is the time delay of the window onset with respect to the time of origin. Comparing (13) with (14) we obtain,

$$\varphi_0 = -\tan^{-1}\left[\frac{\int_0^L F(\tau)\sin\omega\tau\, d\tau}{\int_0^L F(\tau)\cos\omega\tau\, d\tau}\right] + f\left(\frac{\Delta_m}{c} - t_m\right) - \frac{(m-1)}{4} - \varphi_{\text{inst}} + \text{integer} \qquad (15)$$

We shall name φ_0 the *initial phase* of the signal. To derive this phase from the data we must know the epicentral distance Δ_m, the time delay t_m, the phase velocities, and the instrumental phase shift. We have computed the initial phases for the signals of Table 1. A sample of a detailed calculation is shown in Table 3. Phase velocities for G waves were computed from $G_2 - G_4$ E-W [*Toksöz and Ben-Menahem,* 1963] for the period range $125 < T < 333$. For the period range $83 < T < 125$ we used the data of the Mongolian earthquake of December 4, 1957, since the pair $G_1 - G_3$ was not available for computations of phase velocities in the short-period range. The Rayleigh wave velocities were also taken from the data of the Mongolian earthquake.

A comparison between the propagation phases of the various G signals is given in Table 4. The values for the signals that were written by a galvanometer of 180 sec are slightly more negative because of different instrumental phase shift. The over-all fit of the results indicates a good coherence for the pairs $G_1 - G_3$ and $G_2 - G_4$ and hence demonstrates the dependability of the Fourier analysis. The empty spaces in the columns indicate a lower-power band for which the phases were not reliable.

The derivation of the source mechanism is summed up in Tables 5 and 6. We have assumed that the total initial phase is the algebraic sum of the space phase, the time phase, and the propagation phase. The first operation is to subtract the initial phases of, say, G_{n+1} from the initial phase of G_n and check whether the differential phase thus obtained is constant or frequency dependent. In the latter case one can further check whether the differential phase fits the simple theory of a moving strike-slip fault. According to this theory the initial phase due to the fault's motion is given by the expression $-bf/2C(C/V \pm \cos\theta_0)$. The theory thus predicts a phase difference of $b\cos\theta_0/\lambda$ between G_n and G_{n+1}. If the observed differential phase $\delta\varphi_0$ is multiplied by the wavelength λ, the result is the constant $(b\cos\theta_0)$.

We now correct the absolute initial phases of each signal for finiteness and instrument response. The remaining phase is therefore com-

TABLE 3. Detailed Calculation of the Propagation Phase for G_2

f, mc/s	c, km/sec	A*	B†	G_2‡
3.0	5.310	.102	0.917	−0.815
3.2	5.230	.069	0.951	−0.882
3.4	5.166	.059	0.986	−0.927
3.6	5.119	.056	1.021	−0.965
3.8	5.076	.062	1.058	−0.996
4.0	5.037	.072	1.095	−1.023
4.2	5.002	.083	1.133	−1.050
4.4	4.971	.092	1.171	−1.079
4.6	4.942	.108	1.211	−1.103
4.8	4.915	.128	1.251	−1.123
5.0	4.891	.145	1.292	−1.147
5.2	4.869	.161	1.335	−1.174
5.4	4.848	.184	1.378	−1.194
5.6	4.829	.204	1.422	−1.218
5.8	4.810	.236	1.468	−1.232
6.0	4.791	.281	1.515	−1.234
6.2	4.772	.338	1.563	−1.225
6.4	4.754	.398	1.612	−1.214
6.6	4.737	.496	1.662	−1.202
6.8	4.722	.512	1.712	−1.200
7.0	4.711	.534	1.764	−1.230
7.2	4.701	.551	1.815	−1.264
7.4	4.691	.574	1.866	−1.292
7.6	4.685	.558	1.917	−1.359
7.8	4.679	.545	1.967	−1.422
8.0	4.674§	.524	2.016	−1.492
8.2	4.670	.494	2.065	−1.571
8.4	4.662	.518	2.112	−1.594
8.6	4.653	.561	2.159	−1.598
8.8	4.646	.582	2.204	−1.622
9.0	4.639	.608	2.249	−1.641
9.2	4.632	.638	2.293	−1.655
9.4	4.626	.659	2.336	−1.677
9.6	4.620	.683	2.379	−1.696
9.8	4.613	.727	2.421	−1.694
10.0	4.608	.744	2.463	−1.719

* $A = 3.75 + f(33493/C - 7569)$.
† B = Fourier integral phase.
‡ $G_2 = A - B$.
§ Phase velocities for frequencies above 8.0 mc/s are from data of the Mongolian earthquake of December 4, 1957.

posed of a temporal phase (which, although it may be frequency dependent, should be the same for all Love and Rayleigh waves) and the spatial phase. At this stage we make use of Table 2, to equalize all initial phases in such a way that the remaining phase functions will be the same for all the signals. Achieving the balance with four signals such as G_2, G_3, R_2, and R_3 means that there is a harmony between the various details of our source model. Moreover, the final results justify the basic assumption in retrospect.

Following this approach, then, we computed the differential phase $\delta\varphi_0$ for the pairs $R_2 - R_3$ and $G_2 - G_3$. The results, which are shown in Table 5, yielded 470 km for the average of $b \cdot \cos\theta_0$ over the spectral window $80 < t < 250$ sec. The final stage of the calculations is given in Table 6. The finiteness correction was computed for $b = 700$ km and $V_f = 3$ km/sec. The instrumental correction was computed for the horizontal electromagnetic linear strain seismograph with a velocity transducer coupled directly to a galvanometer having a free period of 70 sec at critical damping. The phase response of the strain seismograph is [*Benioff*, 1935]

$$\begin{bmatrix}\text{Rayleigh waves}\\ \text{Love waves}\end{bmatrix} = \begin{bmatrix}\cos^2\alpha\\ -\sin 2\alpha\end{bmatrix} \cdot \exp\left[i\tan^{-1}\left[\frac{2T/T_g}{1-(T/T_g)^2}\right]\right] \quad (16)$$

where α is the ray azimuth, measured positively from the rod's direction, T is the period, and T_g is the period of the galvanometer.

Finally, we must fix the frequency response of the strain seismograph at the limits $T = 0$ and $T = \infty$ under the sign convention adopted in the usual test of the instrument. This is important since we are interested in displacements at the source, and therefore we intend to use the strain seismograph as a displacement recorder. The convention is followed that compression (taken in the Fourier analysis as positive) is equivalent to 'outward from the source' and dilatation is equivalent to 'toward the source.' The instrumental phase shift will then be zero for $T = 0$ and π for $T = \infty$. Hence the instrumental correction is given by $-\pi^{-1}\tan^{-1} T/T_g$. This is true for both Love and Rayleigh waves when the displacement component along the direction of the strained rod is under consideration. However, one should remember that two perpendicular strain rods will register an incoming G wave with opposite polarities [*Benioff and Gutenberg*, 1952]. The previous sign convention (K. Aki, personal communication) can be used in order to determine which of the two components is positive.

Let us now return to Table 6. If we correct the initial phase of the Rayleigh waves R_2 and

TABLE 4.

Demonstration of Phase Coherence of G Wave Signals (N-S components corrected by π for instrumental directional shift)

f, Mc/s	Phase $= N - m/4 + f(\Delta_m/C - t_m)$ − Fourier Phase						
	G_2 E-W 70	G_2 N-S 70	G_2 N-S 180	G_4 N-S 70	G_1 N-S 180	G_3 E-W 70	G_3 N-S 70
3.4	−0.927	−0.836	−0.984	−0.843		−1.156	
3.6	−0.965	−0.884	−1.014	−0.893		−1.216	
3.8	−0.996	−0.925	−1.042	−0.933		−1.263	
4.0	−1.023	−0.961	−1.070	−0.966		−1.315	
4.2	−1.050	−0.996	−1.099	−1.000		−1.363	
4.4	−1.079	−1.033	−1.134	−1.042		−1.423	
4.6	−1.103	−1.064	−1.165	−1.070		−1.492	
4.8	−1.123	−1.092	−1.188	−1.090		−1.608	
5.0	−1.147	−1.121	−1.219	−1.122		−1.700	
5.2	−1.174	−1.151	−1.251	−1.154	−1.932	−1.818	
5.4	−1.194	−1.175	−1.279	−1.177	−2.011	−1.878	
5.6	−1.218	−1.203	−1.314	−1.209	−2.096	−1.928	−2.022
5.8	−1.232	−1.218	−1.340	−1.224	−2.100	−1.956	−2.027
6.0	−1.234	−1.222	−1.353	−1.226	−2.106	−1.966	−2.020
6.2	−1.225	−1.214	−1.352	−1.225	−2.111	−1.959	−2.001
6.4	−1.214	−1.202	−1.344	−1.233	−2.123	−1.950	−1.982
6.6	−1.202	−1.190	−1.329	−1.226	−2.131	−1.939	−1.962
6.8	−1.200	−1.187	−1.320	−1.213	−2.147	−1.937	−1.950
7.0	−1.230	−1.215	−1.342	−1.218	−2.163	−1.978	−1.972
7.2	−1.264	−1.248	−1.368	−1.287	−2.167	−2.019	−1.981
7.4	−1.292	−1.275	−1.390	−1.293	−2.198	−2.043	−2.000
7.6	−1.359	−1.341	−1.453	−1.364	−2.219	−2.114	−2.046
7.8	−1.422	−1.403	−1.561	−1.382	−2.239	−2.174	−2.098
8.0	−1.492	−1.474	−1.587	−1.391	−2.261	−2.243	−2.162
8.2	−1.571	−1.554	−1.665	−1.467	−2.273	−2.326	−2.245
8.4	−1.594	−1.579	−1.685	−1.462	−2.280	−2.335	−2.255
8.6	−1.598	−1.587	−1.679	−1.432	−2.290	−2.323	−2.241
8.8	−1.622	−1.615	−1.690	−1.460	−2.300	−2.343	−2.260
9.0	−1.641	−1.638	−1.691	−1.488	−2.307	−2.364	−2.277
9.2	−1.655	−1.656	−1.686	−1.506	−2.317	−2.384	−2.295
9.4	−1.677	−1.684	−1.690	−1.553	−2.327	−2.427	−2.348
9.6	−1.696	−1.709	−1.692	−1.594		−2.482	−2.447
9.8	−1.694	−1.714	−1.676	−1.592		−2.538	−2.566
10.0	−1.719	−1.746	−1.691	−1.647		−2.660	−2.662

R_2 for the spatial phase of a right lateral couple (Table 2, Figure 4) the residuals will center around $\pi/2$. To obtain similar residuals with the Love waves we shall have to correct it for a left lateral couple (+0.375). This apparent contradiction can be resolved if we assume that the force system was that of a right double couple, such as is shown in Figure 4. The inner ring in this figure shows the quadrant distribution sin 2θ appropriate for the Rayleigh wave radiation from a right lateral couple or a right double couple, whereas the outer ring gives the distribution cos 2θ corresponding to the Love wave radiation from a right double couple. It seems, therefore, that of all simple force systems, the double-couple system is the only one which yields the same time function for the four signals R_2, R_3, G_2, and G_3.

The interpretation of the temporal phase is the next step in this process. The values of the residuals are listed in Table 6 and plotted for G_2 and R_2 in Figure 14. To make these results meaningful we must first estimate the error involved in the evaluation of the initial phases. Since we have practically eliminated the error in the epicentral distance, we need to consider only the error due to inaccuracies in the phase velocities. This is given by

$$d\varphi_0 \approx -\Delta dC/\lambda C \qquad (17)$$

TABLE 5. Derivation of the Fault Length of the Kamchatka Earthquake from the Differential Phases of Love and Rayleigh Waves

		Love Waves					Rayleigh Waves				
f, Mc/s	T, sec	G_2	G_3	$\delta\varphi_0 = G_2 - G_3$	λ, km	$\lambda\,\delta\varphi_0 = b\cos\theta_0$, km	R_2	R_3	$\delta\varphi_0 = R_2 - R_3$	λ, km	$\lambda\,\delta\varphi_0 = b\cos\theta_0$, km
4.0	250.0	−1.023	−1.315	0.292	1259.2	367	−0.500	−0.837	0.337	1229.0	414
4.2	238.1	−1.050	−1.363	0.313	1191.0	373	−0.529	−0.872	0.343	1147.6	394
4.4	227.2	−1.079	−1.423	0.344	1129.8	388	−0.530	−0.917	0.387	1078.9	418
4.6	217.4	−1.103	−1.492	0.389	1074.3	418	−0.467	−0.941	0.474	1018.5	483
4.8	208.3	−1.123	−1.608	0.485	1024.0	496	−0.447	−0.969	0.522	961.5	502
5.0	200.0	−1.147	−1.700	0.553	978.2	541	−0.580	−1.111	0.531	914.0	485
5.2	192.3	−1.174	−1.818	0.644	936.2	603	−0.614	−1.163	0.549	868.3	477
5.4	185.1	−1.194	−1.878	0.684	897.8	614	−0.588	−1.175	0.587	829.8	487
5.6	178.6	−1.218	−1.928	0.710	862.3	612	−0.606	−1.242	0.636	792.1	504
5.8	172.4	−1.232	−1.956	0.724	829.3	600	−0.576	−1.228	0.652	759.6	495
6.0	166.6	−1.234	−1.966	0.732	798.5	584	−0.614	−1.283	0.669	728.7	487
6.2	161.2	−1.225	−1.959	0.734	769.5	565	−0.639	−1.315	0.675	702.6	474
6.4	156.2	−1.214	−1.950	0.736	742.8	547	−0.637	−1.372	0.735	674.8	496
6.6	151.5	−1.202	−1.939	0.737	717.7	529	−0.707	−1.435	0.728	650.0	473
6.8	147.0	−1.200	−1.937	0.737	694.4	512	−0.771	−1.517	0.746	629.6	532
7.0	142.8	−1.230	−1.978	0.748	673.0	503	−0.891	−1.675	0.784	610.0	478
7.2	138.9	−1.264	−2.019	0.755	652.9	493	−0.950	−1.754	0.804	591.2	534
7.4	135.1	−1.292	−2.043	0.751	633.9	476	−1.040	−1.904	0.864	574.2	496
7.6	131.6	−1.359	−2.114	0.754	616.4	465	−1.140	−1.915	0.775	557.4	432
7.8	128.2	−1.422	−2.174	0.752	600.0	451	−1.173	−2.034	0.861	540.9	466
8.0	125.0	−1.492	−2.243	0.751	584.3	439	−1.226	−2.135	0.909	525.6	477
8.2	121.9	−1.571	−2.326	0.752	569.5	428					
8.4	119.0	−1.594	−2.335	0.741	550.0	411					
8.6	116.2	−1.598	−2.323	0.725	541.0	392					
8.8	113.6	−1.622	−2.343	0.721	527.9	380					
9.0	111.1	−1.641	−2.364	0.685	515.4	353					
9.2	108.6	−1.655	−2.384	0.723	503.5	364					
9.4	106.3	−1.677	−2.427	0.750	492.1	369					
9.6	104.1	−1.696	−2.482	0.786	481.2	378					
9.8	102.0	−1.694	−2.538	0.844	470.7	397					
10.0	100.0	−1.719	−2.660	0.941	460.5	433					
10.2	98.0	−1.724	−2.737	1.013	451.2	457					
10.4	96.1	−1.741	−2.802	1.061	442.0	469					
10.6	94.3	−1.756	−2.846	1.090	433.2	472					
10.8	92.6	−1.750	−2.859	1.109	424.6	471					
11.0	90.9	−1.777	−2.863	1.086	416.5	452					
11.2	89.3	−1.793	−2.890	1.097	408.6	448					
11.4	87.7	−1.786	−2.897	1.111	401.1	445					
11.6	86.2	−1.795	−2.925	1.130	393.8	445					
11.8	84.7	−1.837	−3.048	1.211	386.8	468					
12.0	83.3	−1.849	−3.072	1.223	380.0	465					
					Average	465				Average	476

TABLE 6. Derivation of the Temporal Phase Function of the Kamchatka Earthquake from the Absolute Phases of Love and Rayleigh Waves E-W (T_p = 70)

			Love Waves (Spatial correction +0.875)						Rayleigh Waves (Spatial correction +0.375)					
f, mc/s	T, sec	$-\varphi_{inst}$	G_2	Finiteness Correction	Temporal Phase of G_2	G_3	Finiteness Correction	Temporal Phase of G_3	R_2	Finiteness Correction	Temporal Phase of R_2	R_3	Finiteness Correction	Temporal Phase of R_3
3.4	294.1	−0.426	−0.927	0.236	−0.241	−1.156	0.557	−0.149	−0.406	0.236	−0.220	−0.415	0.556	−0.009
3.6	277.7	−0.421	−0.965	0.248	−0.263	−1.216	0.592	−0.170	−0.480	0.246	−0.280	−0.598	0.593	−0.118
3.8	263.1	−0.417	−0.996	0.260	−0.278	−1.263	0.626	−0.179	−0.463	0.256	−0.249	−0.728	0.630	−0.100
4.0	250	−0.413	−1.023	0.272	−0.289	−1.315	0.661	−0.192	−0.500	0.266	−0.272	−0.837	0.667	−0.208
4.2	238.1	−0.409	−1.050	0.284	−0.300	−1.363	0.696	−0.201	−0.529	0.276	−0.287	−0.872	0.704	−0.202
4.4	227.2	−0.405	−1.079	0.296	−0.313	−1.423	0.730	−0.223	−0.530	0.285	−0.275	−0.917	0.741	−0.206
4.6	217.4	−0.401	−1.103	0.308	−0.321	−1.492	0.764	−0.254	−0.467	0.295	−0.198	−0.941	0.778	−0.189
4.8	208.3	−0.397	−1.123	0.321	−0.324	−1.608	0.800	−0.330	−0.447	0.304	−0.165	−0.969	0.815	−0.276
5.0	200	−0.393	−1.147	0.333	−0.332	−1.700	0.833	−0.385	−0.580	0.314	−0.284	−1.111	0.852	−0.277
5.2	192.3	−0.389	−1.174	0.345	−0.343	−1.818	0.868	−0.464	−0.614	0.323	−0.205	−1.163	0.889	−0.288
5.4	185.1	−0.385	−1.194	0.357	−0.347	−1.878	0.903	−0.485	−0.588	0.333	−0.265	−1.175	0.927	−0.258
5.6	178.6	−0.381	−1.218	0.369	−0.356	−1.928	0.937	−0.498	−0.606	0.343	−0.270	−1.242	0.964	−0.285
5.8	172.4	−0.377	−1.233	0.381	−0.354	−1.956	0.972	−0.486	−0.576	0.352	−0.226	−1.228	1.001	−0.229
6.0	166.6	−0.373	−1.234	0.393	−0.339	−1.966	1.006	−0.458	−0.614	0.362	−0.250	−1.283	1.038	−0.243
6.2	161.2	−0.370	−1.225	0.406	−0.313	−1.959	1.041	−0.412	−0.639	0.372	−0.261	−1.315	1.075	−0.234
6.4	156.2	−0.366	−1.214	0.418	−0.287	−1.950	1.075	−0.366	−0.637	0.381	−0.247	−1.372	1.112	−0.251
6.6	151.5	−0.362	−1.202	0.430	−0.259	−1.939	1.110	−0.316	−0.707	0.391	−0.303	−1.435	1.149	−0.273
6.8	147.0	−0.358	−1.200	0.442	−0.241	−1.937	1.144	−0.276	−0.771	0.401	−0.353	−1.517	1.186	−0.314
7.0	142.8	−0.355	−1.230	0.454	−0.256	−1.978	1.179	−0.279	−0.891	0.411	−0.460	−1.675	1.223	−0.432
7.2	138.9	−0.351	−1.264	0.466	−0.274	−2.019	1.214	−0.281	−0.950	0.420	−0.506	−1.754	1.260	−0.469
7.4	135.1	−0.348	−1.292	0.478	−0.287	−2.043	1.248	−0.268						
7.6	131.6	−0.344	−1.359	0.490	−0.338	−2.114	1.283	−0.300						
7.8	128.2	−0.341	−1.422	0.502	−0.385	−2.174	1.317	−0.323						
8.0	125.0	−0.337	−1.492	0.515	−0.439	−2.243	1.352	−0.353						
8.2	121.9	−0.334	−1.571	0.527	−0.503	−2.326	1.386	−0.400						
8.4	119.0	−0.331	−1.594	0.539	−0.511	−2.335	1.421	−0.370						
8.6	116.2	−0.327	−1.598	0.551	−0.499	−2.323	1.455	−0.320						
8.8	113.6	−0.324	−1.622	0.563	−0.508	−2.343	1.490	−0.302						
9.0	111.1	−0.321	−1.641	0.575	−0.512	−2.364	1.524	−0.286						
9.2	108.6	−0.318	−1.655	0.587	−0.511	−2.384	1.559	−0.268						
9.4	106.3	−0.315	−1.677	0.600	−0.517	−2.427	1.594	−0.273						
9.6	104.1	−0.312	−1.696	0.612	−0.520	−2.482	1.628	−0.290						
9.8	102.0	−0.309	−1.694	0.624	−0.503	−2.538	1.663	−0.308						
10.0	100.0	−0.305	−1.719	0.636	−0.513	−2.660	1.697	−0.400						
10.2	98.0	−0.303	−1.724	0.648	−0.504	−2.737	1.732	−0.433						
10.4	96.1	−0.300	−1.741	0.660	−0.506	−2.802	1.766	−0.461						
10.6	94.3	−0.297	−1.756	0.672	−0.506	−2.846	1.801	−0.467						
10.8	92.6	−0.294	−1.750	0.684	−0.485	−2.859	1.835	−0.443						
11.0	90.9	−0.291	−1.777	0.697	−0.496	−2.863	1.870	−0.409						
11.2	89.3	−0.288	−1.793	0.709	−0.497	−2.890	1.904	−0.400						
11.4	87.7	−0.286	−1.786	0.721	−0.475	−2.897	1.939	−0.368						
11.6	86.2	−0.283	−1.795	0.733	−0.470	−2.925	1.973	−0.360						
11.8	84.7	−0.280	−1.837	0.745	−0.497	−3.048	2.008	−0.395						
12.0	83.3	−0.278	−1.849	0.757	−0.494	−3.072	2.043	−0.431						

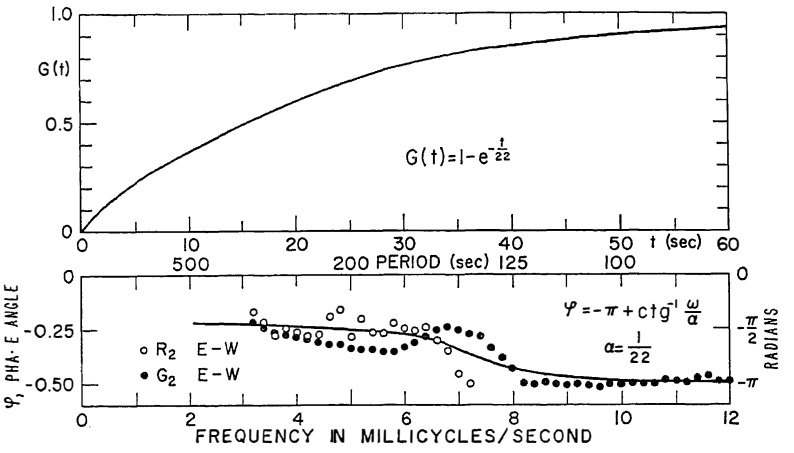

Fig. 14. The observed phase spectrums of the source time function and the reconstructed source time function of the Kamchatka earthquake.

If we take $dC = 0.01$ km/sec, the error in the initial phase is 0.07 circle at $T = 250$ sec, 0.10 circle at $T = 145$ sec, and 0.2 circle at $T = 80$ sec. The phases at shorter periods show very little scatter, which suggests that the actual error was rather small. However, the fact that we used the phase velocities of the Mongolia earthquake for periods shorter than 125 sec does not allow us to accept these results with absolute certainty. We conclude, therefore, that the initial temporal phase of the Kamchatka earthquake is between $-\pi/2$ and $-\pi + \cot^{-1}(\omega/\alpha)$, which is the best fit for the empirical phase data (Figure 14).

We can now invoke causality in order to recover the time function itself from the phases, using the Kramers-Kronig dispersion relations [*Kramers*, 1927; *Kronig*, 1926]. Let $G(t)$ be a causal time function, $G(t) = 0$ for $t < 0$, with a spectrum $g(\omega) \exp[i\beta(\omega)]$. By means of the dispersion relations it is possible to express the amplitude in terms of the phases through the form

$$\ln [g(\omega)] = -\frac{2}{\pi} P \int_0^\infty \frac{y\beta(y)}{y^2 - \omega^2}\, dy \qquad (18)$$

where P stands for the principal value of the integral. For $\beta = -\pi/2$ we obtain $g(\omega) = 1/\omega$ which in turn leads to the unit step function. To find the time function corresponding to the empirical phase $\beta(y) = -\pi + \cot^{-1}(y/\alpha)$ we integrate (18) and obtain $g(\omega) = \alpha/\omega(\alpha^2 + \omega^2)^{1/2}$. The Fourier transform of $g(\omega) \exp[i\beta(\omega)]$ then yields the simple time function.

$$G(t) = 1 - e^{-\alpha t} \qquad (19)$$

This curve is plotted in Figure 14 with $\alpha = 1/22$ as derived from the data.

Auxiliary data. Båth and Benioff [1958] showed that the geographical distribution of the Kamchatka earthquake aftershocks in the period November 1952 to December 1956 were distributed over an area approximately 1030 km long by 240 km wide. *Hutchinson* [1954] studied the aftershock distribution of this earthquake in November 1952. His map, which serves as the basis of our Figure 15 shows an area 675 km long and 240 km wide. The line that passes through the epicenter and bisects the aftershock area lengthwise makes an angle of 140° with the geodesic to Pasadena. These findings, based on Hutchinson's data, are in excellent agreement with our results. We believe that the extension of 1030 km as obtained by Båth and Benioff represents a wider seismic zone which extends beyond the active fault that caused the earthquake of November 4, 1952. It is quite interesting to note that this extension occurred mainly north of the main epicenter. It seems likely that the length of the aftershock zone in a relatively short period following the main shock is a good measure of the active fault during the earthquake. We checked this conjecture for the Mongolia earthquake of December 4,

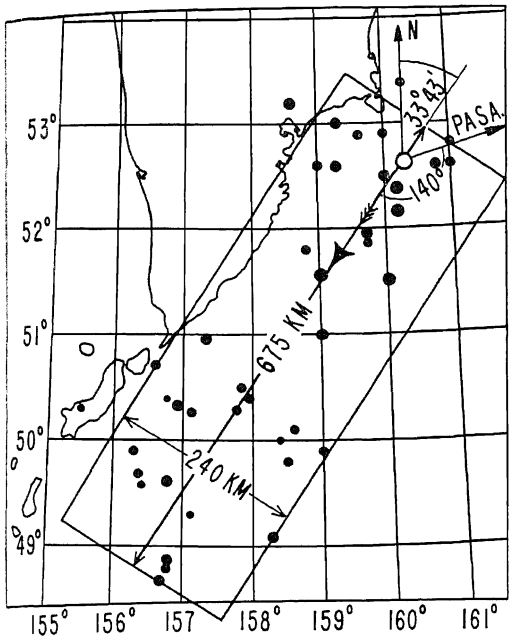

Fig. 15. Aftershock distribution in the month of November 1952 at the source region of the Kamchatka earthquake.

1957 [*Ben-Menahem and Toksöz*, 1962], and found that the aftershock area had reached the length of 500 km seven days after the main shock.

Focal depth. A method of deriving the focal depth from the spectrums of surface waves has not been found yet. One may, however, put an upper bound to the focal depth by the following reasoning: the horizontal Rayleigh component due to a force system with a horizontal component shows a change in the sign of the displacement at a particular critical frequency which depends on the focal depth. For an homogeneous half-space we have the simple relation.

$$h = (0.19) \times \text{critical wavelength} \qquad (20)$$

The phase of the time function of the Kamchatka earthquake did not show a jump of π for periods down to 100 sec. This suggests that the focal depth was less than 80 km. *Hutchinson* [1954] and *Båth and Benioff* [1958] agree on an average focal depth of 60 km.

Conclusion. A source mechanism has been deduced from spectrums of mantle Love and Rayleigh waves from the Kamchatka earthquake of November 4, 1952. The final results are:

Fault length	$b = 700 \pm 50$ km
Rupture speed	$V = 3 \pm 0.25$ km/sec
Angle of fault to station	$\theta = 140° \pm 5°$

The error was evaluated in the following way. We assumed that the experimental error in measuring the product $(b \cos \theta)$ arises mainly from errors in the phase velocities. Since the errors in the initial phases are $d\varphi_0 = dC\ (\Delta_3 - \Delta_2)/TC^2$, the error in the product $\lambda\delta\varphi_0$ will be $dC\ (\Delta_3 - \Delta_2)/C$. With $\Delta_3 - \Delta_2 = 13078$ km and $dC/C \approx \frac{1}{2}$ per cent, we get $d(b \cos \theta_0) \approx 65$ km, which is in good agreement with the difference between $(b \cos \theta_0) = 532$ km, as measured from the amplitudes, and $(b \cos \theta_0) = 470$ km, as measured from the phases. Furthermore, since $d(b \cos\theta_0) = db \cos\theta_0 + bd(\cos\theta_0)$, the error of 65 km in $(b \cos \theta)$ will correspond to an error of about 50 km in b and 5° in the angle. This splitting is quite reasonable, but it is not unique.

We did not have any check on the rupture speed of the present shock, and we therefore adopted an average error which was found by us for the rupture speed of the Alaska earthquake of July 10, 1958. In general, there is a possibility of estimating the average rupture speed of a major earthquake by checking the duration of some phenomena associated with the shock, such as tsunamis, T phases, or air waves.

The unit of stress dislocation seems to be that of a right double couple rather than that of a single right couple.

The time function of the spatial stress dislocation is equal or close to the unit step function.

There is indirect evidence that the focal depth did not exceed 80 km.

Acknowledgments. This research was supported by grant AF-AFOSR-25-63 of the Air Force Office of Scientific Research as part of the Advanced Research Projects Agency project Vela.

We wish to express our thanks to Professor Hugo Benioff for his deep interest in the project. Acknowledgments are also due Professor Frank Press and Dr. Keiiti Aki for a critical reading of the manuscript. The time series analysis and azimuth-distance computer programs used in the data analysis were written by Dr. Shelton S. Alexander.

References

Aki, K., Accuracy of the Rayleigh wave method for studying the earthquake mechanism, *Bull. Earthquake Res. Inst., Tokyo Univ., 40,* 91–105, 1962.

Alexander, S. S., Surface wave propagation in the western United States, Ph.D. thesis, California Institute of Technology, Pasadena, 1963.

Båth, M., and H. Benioff, The aftershock sequence of the Kamchatka earthquake of November 4, 1952, *Bull. Seismol. Soc. Am., 48,* 1–15, 1958.

Benioff, H., A linear strain seismograph, *Bull. Seismol. Soc. Am., 25,* 283–309, 1935.

Benioff, H., Long waves observed in the Kamchatka earthquake of November 4, 1952, *J. Geophys. Res., 63,* 589–593, 1958.

Benioff, H., and B. Gutenberg, The response of strain and pendulum seismographs to surface waves, *Bull. Seismol. Soc. Am., 43,* 229–237, 1952.

Ben-Menahem, A., Radiation pattern of seismic surface waves from simple models of fault planes, 1, Rayleigh waves, *Project Vela Rept.,* Seismological Laboratory, California Institute of Technology, Pasadena, 1960.

Ben-Menahem, A., Radiation of seismic surface waves from finite moving sources, *Bull. Seismol. Soc. Am., 51,* 401–435, 1961.

Ben-Menahem, A., and M. Nafi Toksöz, Source mechanism from spectra of long-period seismic surface waves, 1, The Mongolian earthquake of December 4, 1957, *J. Geophys. Res., 67,* 1943–1955, 1962.

Bomford, G., *Geodesy,* Clarendon Press, Oxford, 1952.

Brune, J., J. Nafe and L. Alsop, Polar phase shift of surface waves on a sphere, *Bull. Seismol. Soc. Am., 51,* 247–257, 1961.

Bullen, K. E., *Introduction to Theoretical Seismology,* Cambridge University Press, 1947.

Ewing, M., and F. Press, Mantle Rayleigh waves from the Kamchatka earthquake of November 4, 1952, *Bull. Seismol. Soc. Am., 44,* 471–479, 1954.

Haskell, N. A., Radiation pattern of Rayleigh waves from a fault of arbitrary dip and direction of motion in a homogeneous medium, *Bull. Seismol. Soc. Am., 53,* 619, 1963.

Hodgson, J. H., Direction of faulting in some of the larger earthquakes of the North Pacific, 1950–1953, *Publ. Dominion Obs., Ottawa, Ont., 17*(10), 1956.

Hutchinson, R. O., The Kamchatka earthquake of November 1952, *Earthquake Notes, 25*(3–4), 37–41, 1954.

Kramers, H. A., La diffusion de la lumiere par les atomes, *Atti Congr. Intern. Fisica, Como, 2,* 545–557, 1927.

Kronig, R., On the theory of the dispersion of X-rays, *J. Opt. Soc. Am., 12,* 547–557, 1926.

Satô, Y., Attenuation, dispersion and the wave guide of the *G*-wave, *Bull. Seismol. Soc. Am., 48,* 231–251, 1958.

Toksöz, M. N., and A. Ben-Menahem, Velocities of mantle Love and Rayleigh waves over multiple paths, *Bull. Seismol. Soc. Am., 53,* 741–764, 1963.

(Manuscript received April 5, 1963; revised June 25, 1963.)